

Physics 357: Second Harmonic Generation

Eliseu Antonio Kloster Filho, Evan McLoughlin

(Dated: October 18, 2023)

Non-linear optics describes the behavior of light when the medium's polarization density is related to the electric field through more than just first-order contributions. In this experiment, we investigate various aspects of a non-linear optical phenomenon called Second Harmonic Generation (SHG). This involves exciting a 40 mm long Poled Lithium Niobate (PPLN) crystal with a 1560 nm laser so that 780 nm light is generated due to the crystal's non-linear response to light. We find that the frequency doubled power is related to the input polarization angle 2θ and input power Q_{in} by $Q_{\text{out}} \propto \sin^4(2\theta)$ and $Q_{\text{out}} \propto Q_{\text{in}}^2$. We also obtain bandwidth acceptance ranges for the crystal's temperature ($\delta T = 2.9 \pm 0.1$ °C) and laser wavelength ($\delta\lambda = 0.299 \pm 0.003$ nm). Moreover, we find good agreement between our experimental results and theoretical predictions.

I. INTRODUCTION

Optical phenomena have been observed and studied for thousands of years, as can be confirmed by archaeological finds of human-made lenses dating from as early as 2000 BC [1]. Still, the study of light and its interaction properties has not stopped evolving. Johannes Kepler wrote his treatise about optics in the early 17th century [2]. Isaac Newton theorized about the nature of light and published *Opticks* in the early 18th century [3]. Maxwell finished his classical theory of electromagnetism in the late 19th century [4]. More recently, lasers were invented. First described as "a solution looking for a problem," they are now useful in research, medicine, industry, and a variety of other fields [5]. In particular, they are a useful tool in the study of non-linear optics.

A. Second-order Non-linear Optical Processes

Non-linear optics are distinguished by responses to an applied optical field by a system that depends on the strength of the applied field in a non-linear manner [6]. For example, when subject to an electric field E_i , the atomic or molecular dipoles of many materials align in such a way that the resulting polarization density vector P_i is proportional to E_i , as seen[7] in Equation 1.

$$P_i = \epsilon_0 \chi_{ij}^{(1)} E_j \quad (1)$$

Although χ_{ij} is a rank-2 tensor in general, for isotropic materials we can write $\chi_{ij} = \delta_{ij} \chi_e$, with scalar χ_e . This response differs, however, with the structure of the materials to which the electric field is applied. Non-linear materials demonstrate polarization that depends on higher-order terms, as described[8] by the following series expansion:

$$P_i = \sum_{n \geq 1} P_i^{(n)} = \epsilon_0 \chi_{ij}^{(1)} E_j + \epsilon_0 \chi_{ijk}^{(2)} E_j E_k + \dots \quad (2)$$

The study of second order nonlinear optics is simply the investigation of materials that have negligible $P_i^{(n)}$ for $n \geq 3$. In particular, when a beam of monochromatic

light of frequency ω travels through a second order non-linear dielectric, part of it will be converted into light of frequency 2ω via radiation generated by the oscillating dipoles in the material. This process is called frequency doubling, or second harmonic generation (SHG). Although conceptually simple, very high irradiance beams are required to observe the nonlinearity effect, which means lasers must be used to study SHG. To analyze this effect further, assume the electric field of the laser is a plane wave with frequency ω_1 propagating in the \hat{x} direction and polarized along the z direction:

$$\vec{E}_1 = \vec{E}(\omega_1) e^{-i\omega_1 t} + \vec{E}(-\omega_1) e^{i\omega_1 t} = \vec{A}(\omega_1) e^{i(k_1 x - \omega_1 t)} + \vec{A}(-\omega_1) e^{-i(k_1 x - \omega_1 t)} \quad (3)$$

The polarization condition implies $A_x = A_y = 0$, so from now on we consider E and A to be the z components of the corresponding vector quantities. Using Equation 2, we find an expression for $P_i^{(2)}$:

$$P_i^{(2)} = \epsilon_0 \chi_{i33}^{(2)} (E(\omega_1) e^{-i\omega_1 t} + \text{c.c.})^2 \quad (4)$$

If we let $P = \sum_{n \in \mathbb{Z}} P(\omega_n) e^{-i\omega_n t}$, we find that for appropriate d_{eff} we can write $|\vec{P}^{(2)}(2\omega_1)| = P^{(2)}(2\omega_1)$ as:

$$P^{(2)}(2\omega_1) = 2\epsilon_0 d_{\text{eff}} E(\omega_1)^2 \quad (5)$$

Since the wave propagates along x , and only the z components of the fields are of interest, we can investigate the problem using the one-dimensional in-homogeneous wave equation for a lossless and dispersionless medium:

$$\frac{\partial^2 E_2}{\partial x^2} - \frac{n_2^2}{c^2} \frac{\partial^2 E_2}{\partial t^2} = \mu_0 \frac{\partial^2 P_2^{(2)}}{\partial t^2} \quad (6)$$

Where the subscript 2 refers to the doubled frequency (e.g. $\omega_2 = 2\omega_1$). If we assume the amplitudes are slowly varying compared to the actual oscillations, we can use the slowly varying envelope approximation (SVEA) to neglect the second derivatives of the electric field amplitudes in Equation 6:

$$\left| \frac{d^2 A(2\omega_1)}{dx^2} \right| \ll \left| k_2 \frac{dA(2\omega_1)}{dx} \right| \quad (7)$$

Thus, using $n_2^2 \omega_2^2 / c^2 = k_2^2$ and this approximation:

$$\begin{aligned} \frac{\partial^2 E_2}{\partial x^2} - \frac{n_2^2}{c^2} \frac{\partial^2 E_2}{\partial t^2} &= e^{i(k_2 x - \omega_2 t)} \left(\frac{\partial^2 A(2\omega_1)}{\partial x^2} + \right. \\ &\quad \left. 2ik_2 \frac{\partial A(2\omega_1)}{\partial x} - k_2^2 A(2\omega_1) \right) + \frac{n^2 \omega_2^2 A(2\omega_1)}{c^2} e^{i(k_2 x - \omega_2 t)} = \\ &e^{i(k_2 x - \omega_2 t)} \left(\frac{\partial^2 A(2\omega_1)}{\partial x^2} + 2ik_2 \frac{\partial A(2\omega_1)}{\partial x} \right) = \\ &e^{i(k_2 x - \omega_2 t)} 2ik_2 \frac{\partial A(2\omega_1)}{\partial x} = \mu_0 \frac{\partial^2 P_2^{(2)}}{\partial t^2} \quad (8) \end{aligned}$$

If we take the time derivative of $P_2^{(2)} = e^{-i\omega_2 t} P^{(2)}(2\omega_1)$:

$$\frac{\partial^2 P_2^{(2)}}{\partial t^2} = -2\omega_2^2 \epsilon_0 d_{\text{eff}} A(\omega_1)^2 e^{i(k_2 x - \omega_2 t)} \quad (9)$$

Plugging this expression back into Equation 8 and rearranging, we obtain:

$$\frac{\partial A(2\omega_1)}{\partial x} = \frac{id_{\text{eff}} \omega_2}{n_2 c} A(\omega_1)^2 e^{i(2k_1 - k_2)} \quad (10)$$

While second harmonic generation is the main focus of this experiment, it should also be noted that second order polarization can lead to other frequency-modifying processes. For example, consider a laser that contains two components of different frequencies ω_1 and ω_2 in the scalar field approximation, as in Equation 11.

$$E = E_1(\omega_1) e^{-i\omega_1 t} + E_2(\omega_2) e^{-i\omega_2 t} + \text{c.c.} \quad (11)$$

Assuming $P^{(2)}(t) = \epsilon_0 \chi^{(2)} E^2(t)$ (scalar field approximation), the second order polarization is given by Equation 12.

$$\begin{aligned} P^{(2)} &= 2\epsilon_0 \chi^{(2)} [E_1^* E_1 + \text{c.c.}] + \\ &\epsilon_0 \chi^{(2)} [E_1^2 e^{-2i\omega_1 t} + E_2^2 e^{-2i\omega_2 t} + 2E_1 E_2 e^{-i(\omega_1 + \omega_2)t} + \\ &\quad 2E_1 E_2^* e^{-i(\omega_1 - \omega_2)t} + \text{c.c.}] \quad (12) \end{aligned}$$

As this equation shows, the polarization has components with the doubled frequencies as well as components with frequencies that are the sum and difference of the laser's original constituent frequencies. The additive and subtractive processes are called, respectively, sum-frequency generation (SFG) and difference-frequency generation (DFG). These second-order processes are summarized in Table I. Sum-frequency generation can be used to produce tunable ultraviolet light by inputting a combination of a fixed frequency visible laser and a tunable frequency visible laser into a non-linear medium. The same can be done to produce tunable infrared light using difference-frequency generation [6].

B. Phase Matching

In order for the second harmonic generation process to produce frequency-doubled radiation at an appreciable

TABLE I: Summary of Second-order Non-linear Optical Processes

Process	Frequency	Amplitude
SHG	2ω	$\epsilon_0 \chi^{(2)} E^2$
SFG	$\omega_1 + \omega_2$	$2\epsilon_0 \chi^{(2)} E_1 E_2$
DFG	$\omega_1 - \omega_2$	$2\epsilon_0 \chi^{(2)} E_1 E_2^*$

power, it is necessary for the interacting optical fields to interfere constructively. The difference in phase velocity between the polarization field and the frequency-doubled field it generates leads to an increasing phase disparity and to destructive interference. The phase velocity difference results from the material's frequency-dependent index of refraction. Naturally, phase matching is a concern for SFG and DFG as well, but only the phase matching conditions in the SHG case will be described here. If the initial plane wave E_1 that leads to the polarization has a frequency of ω_1 , its wavevector in the non-linear material is $k_1 = n_1 \omega_1 / c$. This wave forces a polarization wave $P_1^{(2)}$ with frequency $\omega_2 = 2\omega_1$ and wavevector $2k_1$, which, because it is forced by E_1 , is determined by n_1 , the index of refraction at frequency ω_1 . The free second harmonic wave E_2 radiated by the polarization has wavevector $k_2 = n_2 \omega_2 / c$, which is determined by n_2 , the index of refraction at frequency ω_2 . The phase shift between $P_1^{(2)}$ and E_2 reaches π after a distance

$$l_c = \frac{\pi}{k_2 - 2k_1} = \frac{\lambda}{4(n_2 - n_1)} \quad (13)$$

This equation gives the coherence length l_c and emphasizes that the phase shift is the result of the index of refraction n being frequency dependent. Beyond l_c , the polarization and second harmonic waves interfere destructively. The direction of power flow is determined by the phase shift between $P_1^{(2)}$ and E_2 , and it changes sign every coherence length. Without phase matching, there is no increase in average power across the length of the non-linear material.

A perfectly phase-matched interaction involves the complete elimination of the phase shift. In this case, the power flows in one unchanging direction, and it increases across the length of the material (remember that P is the polarization *density*). One approach to eliminating the phase shift is birefringent phase matching (BPM), where the material has indices of refraction dependent on the direction of the polarization of the optical fields, and this dependency is leveraged to compensate for the phase shift. Careful manipulation of the angles between the crystal's optic axes and the direction of propagation of incident light is one approach to BPM. There are two important limitations to BPM. The first is the requirement for the non-linear material to have birefringence, and there are in fact non-linear materials that have no birefringence [6]. The second limitation is that the birefringence, that is, the disparity of refractive indices between ordinarily and extraordinarily polarized light, may

not be sufficient to compensate for the disparity in refractive indices at different frequencies. Essentially, BPM limits phase matching to certain materials and certain frequencies.

Another method to deal with the phase mismatch between the polarization and second harmonic fields is quasi-phase matching (QPM). In QPM, the sign of the non-linear susceptibility $\chi^{(2)}$ is inverted every coherence length l_c , so that the phase of the polarization field immediately increases by π and the phase shift is "reset." This ensures that, although the phase shift is not eliminated, the polarization and second harmonic fields will never interfere destructively. The inversion of $\chi^{(2)}$ is accomplished in fabrication, for example, by assembling a series of wafers of non-linear material, each having a width l_c , and rotating every second wafer 180° . In ferroelectric crystals, QPM is done by creating domains of periodically reversed spontaneous polarization [9]. Quasi-phase matching can be represented as setting the non-linear coupling $d(z)$ to a square wave, where the sign is inverted every $\Lambda/2$ across the non-linear material. Λ is called the poling period, and it is chosen based on the coherence length of the second-order process the material is designed for: $\Lambda = 2ml_c$ where m is an odd integer, the order of quasi-phase matching.

$$d(z) = d_{\text{eff}} \text{sign} \left[\cos \left(\frac{2\pi z}{\Lambda} \right) \right] \quad (14)$$

This can be written as Fourier series

$$d(z) = d_{\text{eff}} \sum_{m=-\infty}^{\infty} \frac{2}{m\pi} \sin(m\pi/2) e^{ik_Q m z} \quad (15)$$

where $k_Q m = 2\pi m/\Lambda$. Assuming a particular m term in this series dominates, and making a slowly varying amplitude approximation, the wave equation becomes

$$\frac{\partial A(2\omega_1)}{\partial x} = \frac{i\omega_2 d_m}{n_2 c} A(\omega_1)^2 e^{i\Delta k_Q z} \quad (16)$$

where $d_m = d_{\text{eff}} \frac{2}{m\pi} \sin(m\pi/2)$ and $\Delta k_Q = 2k_1 - k_2 + k_{Qm}$. For first-order ($m = 1$) QPM, where the material is inverted every coherence length, the non-linear coupling is $d_1 = (2/\pi)d_{\text{eff}}$, meaning the efficiency of SHG is reduced by a factor of $2/\pi$ compared to perfect phase matching. Despite the reduction in efficiency, QPM is unfettered by the limitations of BPM: It allows efficient SHG at a wider range of frequencies, it can be realized in any material into which periodic inversion can be fabricated, birefringent or not, and it allows the respective polarizations of incident and second harmonic fields to be chosen freely, allowing access to *any* non-linear coefficient in the susceptibility tensor.

C. Applications of SHG

As with the other non-linear processes, SHG can provide access to tunable light at frequency ranges that

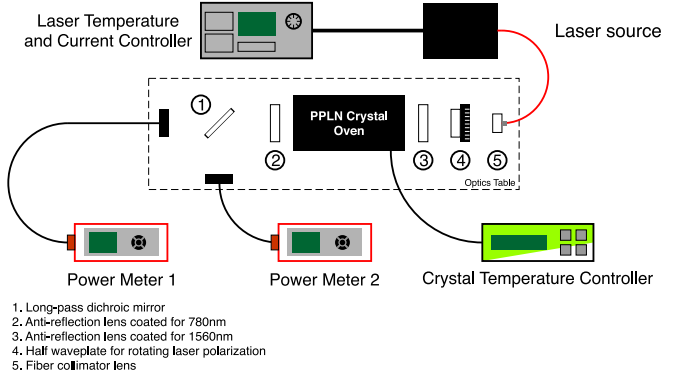


FIG. 1: Diagram of SHG Apparatus

could otherwise be inaccessible. SHG allows the generation of frequencies that are either impossible or very expensive to create by doubling frequencies that are cheaper and more readily available. In situations where high amounts of power at a specific frequency are needed, it may be easiest or necessary to use SHG rather than producing light at that frequency directly. In particular, SHG is used to double the frequency of 1064 nm light into green 532 nm light in laser pointers, and to create high power 780 nm lasers from 1560 nm input for use in experiments with low-temperature rubidium atoms. The 780 nm wavelength is important for these experiments because it is the wavelength of rubidium's D_2 transition [10].

II. APPARATUS

The experimental apparatus is designed to send a diode laser at nominal wavelength 1560 nm through a periodically poled lithium niobate (PPLN) crystal in order to produce light at a wavelength of $1560/2 = 780$ nm. The frequency doubled light is then separated from the 1560 nm wavelength laser light when the two optical fields encounter a long-pass dichroic mirror which reflects 780 nm light and transmits 1560 nm light. Finally, the 780 nm light is measured by a calibrated optical power meter. The components are listed in the order they become involved in the experimental process. The entire apparatus is depicted in Figures 1 and 2.

A. 1560 nm Diode Laser

A current drives a diode laser which is output by an optical fiber. The laser is connected to a temperature and current controller (Figure 3). The controller, allows the current driving the laser to be set with 0.1 mA precision, allows the temperature to be set with 0.01 $^\circ\text{C}$ precision, enables and disables feedback cooling, and allows the laser to be turned on or off by a button and lock. The laser is capable of power up to 20 mW, and its



FIG. 2: Photograph of SHG Apparatus



FIG. 3: Oven temperature controller (top) and laser temperature and current controller (bottom).

driving current can be up to 128.00 mA. The feedback cooling was enabled for the entire duration of the experiment to prevent the laser from overheating, and the laser temperature remained in the 20–35 °C range. Both the current and the temperature have a measurable influence on the frequency of the laser, with the temperature control allowing the laser's frequency to be tuned. The laser's wavelength changes by 0.1 nm per degree Celsius.

B. Half Waveplate

The first component encountered by the laser is a half waveplate. This waveplate polarizes the laser linearly at various angles. The waveplate is capable of rotating in a complete circle, and lines on its cylindrical surface mark every 2 degrees. The PPLN crystal transmits light depending on the vertical component of the incident light, so the waveplate angle and the polarization angle corresponding to it have a significant effect on the intensity of the second harmonic field. This effect will be explained in detail in Section IV.

C. First Lens

After the laser passes through the waveplate and becomes polarized, it encounters a lens that is anti-reflection coated for 1560 nm light. This lens focuses the laser so that it becomes narrowest at the center of the PPLN crystal.

D. Oven and PPLN Crystal

The PPLN crystal, created by Coversion, is mounted in a temperature-controlled oven, which is on a translation stage. The oven includes a heater with a variable 3.6 – 15 W power rating and a PT100 resistance temperature sensor. It is cabled and connected to a temperature controller, shown in Figure 3. Using the controller, the temperature can be set with .01 °C precision. The oven and crystal can tolerate temperatures up to 200 °C and changes in temperature less than 25 °C per minute. Periodically poled lithium niobate is an engineered, quasi-phase matched, and non-linear ferroelectric crystal. The orientation, and thus the polarization, of the crystal is periodically inverted. The particular crystal in this experiment is a 40 nm 5% MgO doped PPLN crystal. The second-order polarization of lithium niobate is given by Equation 17[11].

$$\begin{pmatrix} P_x^{(2)} \\ P_y^{(2)} \\ P_z^{(2)} \end{pmatrix} = 2 \begin{pmatrix} 0 & 0 & 0 & 0 & d_{31} & -d_{22} \\ -d_{22} & -d_{22} & 0 & d_{31} & 0 & 0 \\ d_{31} & d_{31} & d_{33} & 0 & 0 & 0 \end{pmatrix} \begin{pmatrix} E_x^2 \\ E_y^2 \\ E_z^2 \\ 2E_z E_y \\ 2E_z E_x \\ 2E_x E_y \end{pmatrix} \quad (17)$$

Where the 2D matrix contains the same information as the susceptibility tensor $\chi^{(2)}$, but there are are much less components due to various symmetry conditions. The MgO:PPLN crystal typically has an effective non-linear coefficient $d_{\text{eff}} = 14 \text{ pm/V}$. The refractive index of the crystal varies with frequency and the temperature of the crystal. The refractive index is given by a temperature dependent Sellmeier equation.

$$n_e^2 = a_1 + b_1 f + \frac{a_2 + b_2 f}{\lambda^2 - (a_3 + b_3 f)^2} + \frac{a_4 + b_4 f}{\lambda^2 - a_5^2} - a_6 \lambda^2 \quad (18)$$

TABLE II: MgO:PPLN Sellmeier Coefficients

a_1	5.756
a_2	0.0983
a_3	0.2020
a_4	189.32
a_5	12.52
a_6	1.32E-2
b_1	2.860E-6
b_2	4.700E-8
b_3	6.113E-8
b_4	1.516E-4

The equation pertains to extraordinarily polarized light, as having all the optical fields e-polarized realizes the greatest SHG efficiency. λ is given in micrometers. f is the temperature dependent parameter, where T is the temperature in degrees Celsius.

$$f = (T - 24.5)(T + 843.97) \quad (19)$$

The Sellmeier coefficients are given in Table II. Ordinarily, the high indices of refraction for the crystal would lead to significant losses due to reflection, but the input and output facets of the PPLN crystal are anti-reflection coated, so reflection is kept below 1% at each end. Undoped PPLN has slightly different Sellmeier coefficients compared to the MgO:PPLN crystal used in this experiment. The addition of 5% MgO to PPLN maintains a high non-linear coefficient while providing increased optical and photorefractive resistances, allowing for higher damage thresholds and the ability to use the crystal at temperatures below 100 degrees Celsius.

E. Second Lens

The second lens is AR coated for 780 nm light and focuses the two free optical fields emerging from the PPLN crystal.

F. Long-pass Dichroic Mirror

The long-pass dichroic mirror is used to separate the 1560 nm laser from the 780 nm light generated in the crystal. The longer wavelength of light is transmitted through this mirror, but the second harmonic light is reflected.

G. Power Meters

Two identical, highly sensitive power meters are used to measure the power of the light as each frequency of light completes its path through the apparatus. The



FIG. 4: Power Meter 1 (right) and 2 (left)

power meters include settings like range of power detected, measurement representation, units, and wavelength entry. Power Meter 1 was set to measure 1560 nm light and displayed power in units of milliwatts with .01 mW precision. Power Meter 2 was set to measure 780 nm light in units of microwatts, with .01 μ W precision. The power meters are shown in Figure 4.

Over the course of the experiment, the apparatus has stayed largely unaltered. Power Meter 1, however, was added only when the effect of the magnitude of current on the output power was being measured. This was done so that the power of first harmonic light could also be related to the amount of current driving the laser, and that the power of 1560 nm and 780 nm light could be compared.

III. MEASUREMENTS AND DATA ANALYSIS

The task of the experiment is to measure the effects of affecting several parameters on the power and efficiency of second harmonic generation. Such parameters include the polarization of the incident light, the amount of current driving that light, the temperature of the PPLN crystal, and the temperature of the laser. Measurements of the power of second harmonic light as these parameters are varied give insight about the SHG process and allow it to be optimized to achieve the greatest level of efficiency.

A. Waveplate Angle/Incident Light Polarization

The particular PPLN crystal used to double the frequency of 1560 nm laser light causes the amount of SHG light produced to depend on the vertical component of the incident light. The half waveplate encountered by the laser before it is focused into the crystal polarizes

the laser linearly, with the angle at which the light is polarized being twice the angle of the waveplate. To achieve the highest power measurement by Power Meter 2, the current on the laser controller was set to the maximum 128.0 mA. The crystal temperature was set to 104.50 °C, and the laser temperature to 24.20 °C. 150 data points over 5 trials investigating the relationship between waveplate angle and second harmonic power are summarized in Figure 5. From theory, we expect the doubled power $Q_{2\omega}$ to relate to the polarization angle θ by $Q_{2\omega} \propto \sin^4(2\theta)$. This is because $Q_{2\omega} \propto A_{2\omega}^2$ and $A_{2\omega} \propto A_\omega^2$ from Equation 10 (assuming constant A_ω). Moreover, $A_\omega \propto \sin(2\theta)$ by the working principles of a half waveplate.

Since we always measured power at the exact same polarization angles, the 5 trials were combined into one data set, and the standard deviation was taken into consideration in the model fitting process. Specifically, we fit models that minimize the χ^2 statistic in Equation 20, where y, x, σ are the model's output, observed data, and standard deviation, respectively.

$$\chi^2 = \sum_i \frac{(y_i - x_i)^2}{\sigma_i^2} \quad (20)$$

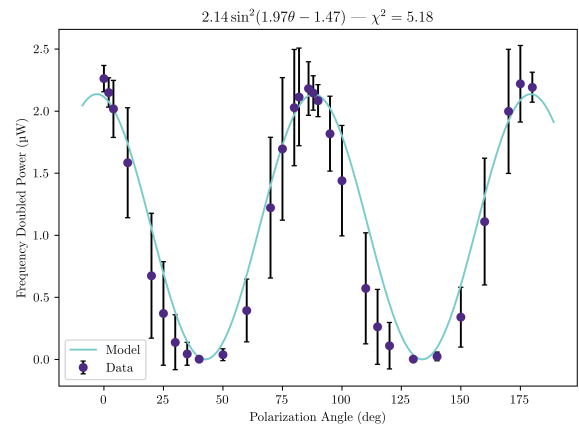
We three different models and confirm that the $\sin^4(2\theta)$ has the smallest χ^2 , as expected.

B. Laser Current

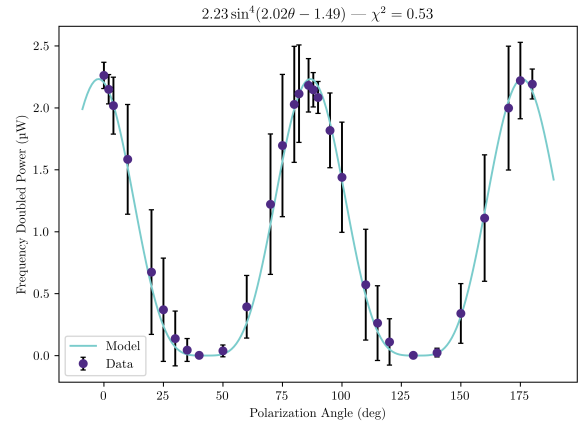
The current has a notably complex effect on the second harmonic output power. Not only does the power depend on the square of the current, but the current also affects the frequency of the diode laser. Because the power meters measure the power at specific frequencies, and deviations from the wavelengths for which the PPLN crystal is designed leads to a loss in efficiency, changing the current results in power measurements that are affected by changes in both current and laser frequency. Our series of measurements allows for this complication, and that's why the effect of laser current on second harmonic power does not really fit a power law (as would be expected if the laser frequency didn't drift with current). Determining that the angle producing the highest second harmonic power is roughly 357 degrees, the waveplate remained at that optimal angle. The crystal temperature was increased to 105.60 °C, while the laser temperature remained at 24.20 °C. The effects of laser current, as set by the laser controller, on both the 1560 nm power and second harmonic power, were then measured. We did 85 measurements over 5 trials, as shown in Figure 7.

C. Input Power and Doubled Power

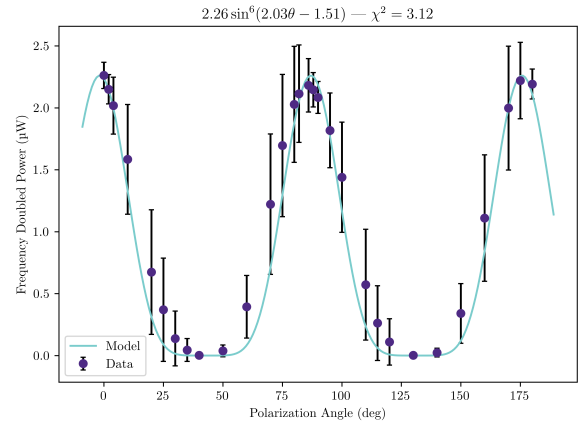
To change the input power we need to change the laser current. However, if we only did that, we would run into



(a) $A = 2.13 \pm 0.05$, $B = 1.97 \pm 0.02$, $C = -1.47 \pm 0.05$



(b) $A = 2.23 \pm 0.02$, $B = 2.02 \pm 0.01$, $C = -1.49 \pm 0.02$



(c) $A = 2.26 \pm 0.04$, $B = 2.02 \pm 0.02$, $C = -1.51 \pm 0.03$

FIG. 5: Data and the corresponding best fit curves for the model represented by $Q(\theta) = A \sin^n(B\theta + C)$ ($n = 2, 4, 6$, respectively). Error bars represent the standard deviation across the 5 measurement trials.

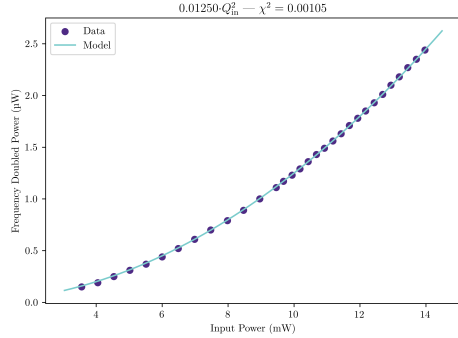
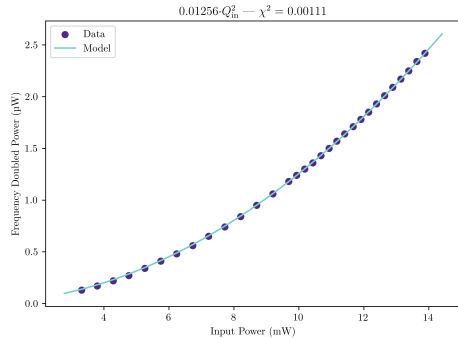
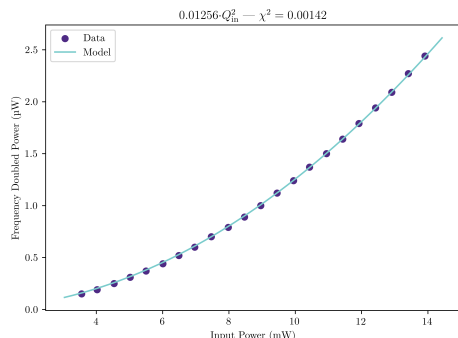
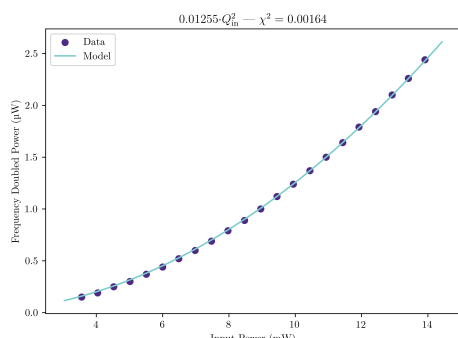
(a) $A = 0.01249 \pm 0.00001$ (b) $A = 0.01255 \pm 0.00001$ (c) $A = 0.01255 \pm 0.00002$ (d) $A = 0.01255 \pm 0.00002$

FIG. 6: Data and the corresponding best fit curves for the model represented by $Q_{\text{out}} = A \cdot Q_{\text{in}}^2$. Each plot represents one of the four trials done for this experiment.

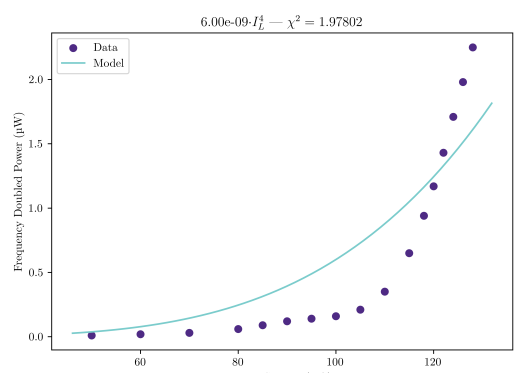
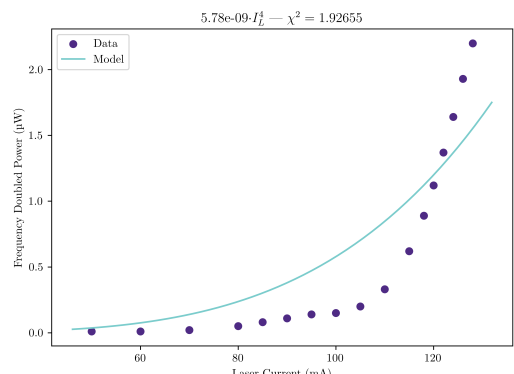
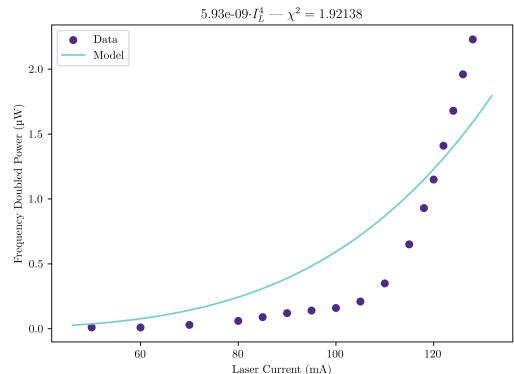
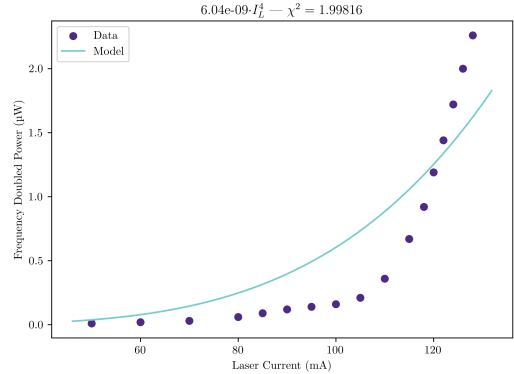


FIG. 7: Data and corresponding best fit curves for the model represented by $Q_{\text{out}} = A \cdot I_L^4$. Each plot represents one of the four trials.

the same problems as in the previous section. A better way to quantify how the 1560 nm laser power affects the 780 nm power is to adjust input power while simultaneously adjusting the laser temperature to maximize the doubled power for each specific data point. By doing this, we guarantee, to an approximation, that the frequency will be the same across all measurements. For this procedure, we used both power meters (one for the input power, one for the doubled power). In total, 86 points of data over 4 trials were collected. The results are summarized in Figure 6. Beyond the $Q_{\text{out}} \propto Q_{\text{in}}^2$, we also tried to fit higher order polynomials and observed that all but the Q_{in}^2 coefficients were negligibly small. This fact, combined with the extremely low χ^2 values for the quadratic fit support the theoretical prediction. We combined the trials using the arithmetic mean of them. The uncertainty in the mean as σ/\sqrt{N} , where σ is the standard deviation of the individual uncertainties and N is the total number of trials. For Q_{out} in μW and Q_{in} in mW , we obtain the experimental result in Equation 21.

$$Q_{\text{out}} = (0.012541 \pm 0.000002)Q_{\text{in}}^2 \quad (21)$$

D. PPLN Crystal Temperature

At the optimal current, the laser temperature that maximized the second harmonic power was found to be approximately 25.91°C, so the laser temperature was set to that value while the effects of the crystal temperature were measured. The current remained at its maximum and the waveplate angle at 357 degrees. Under these conditions, the effects of the crystal temperature, as set by the oven controller, were investigated. Although the crystal has a wide range of temperatures it can tolerate, the rate at which the temperature is changed and the amount of time required for the roughly 400 mm³ crystal to thermalize completely were important considerations. Attempts to change the temperature well below and above its usual 100 to 110 degrees led to several very imprecise measurements unworthy of inclusion in this report, but they did indicate an area of interest in the relatively narrow 100 to 110 degree range. Focusing on that range, each measurement was made after allowing five, and later four, minutes to pass, during which the crystal thermalized to the temperature set on the oven controller. The 5 trials and 96 measurements of second harmonic power over the ten degree range of crystal temperatures are summarized in Figure 8. In fact, it is difficult to model the effect of the crystal temperature with any simple function. Near the maximum power, though, the temperature affects output power in an approximately Gaussian manner. To judge our experimental results, we use the theoretical prediction of the full width at half maximum (FWHM) given by Equation 22, which was derived by Fejer et al.

$$\delta T = \frac{0.4429\lambda}{L} \left| \frac{\partial \Delta n}{\partial T} + \alpha \Delta n \right|^{-1} \quad (22)$$

For this experiment $\lambda = 1560\text{nm}$, $\Delta n = n_{780} - n_{1560}$ (taken from Equation 18), $L = 40\text{mm}$, and the coefficient of linear thermal expansion is $\alpha = L^{-1} \frac{\partial L}{\partial T} \approx 10^{-5}$. The final theoretical prediction is then:

$$\delta T = 1.51 \text{ } ^\circ\text{C} \quad (23)$$

We can compare it to our best estimate of the FWHM:

$$\delta T = 2.9 \pm 0.1 \text{ } ^\circ\text{C} \quad (24)$$

E. Laser Temperature and Frequency

The optimal temperature for the PPLN crystal was found to be 105.00 °C, so the crystal remained at that temperature during the investigation of laser temperature. The waveplate angle remained at 357 degrees and the input current at 128.0 mA. The laser temperature is selected by the laser controller, and it is a quantity of interest because it affects the laser's frequency. As previously mentioned, the laser's wavelength changes by 0.1 nm per degree Celsius. The frequency affects the output power due to both the power meter measuring at a specific frequency and its effect on the phase shift and therefore the efficiency of SHG. Unlike the crystal temperature, the laser temperature requires much less time to stabilize, so measurements of power were made almost immediately after the temperature was set. Measurements were constrained to the 20 to 35 degree range. The 5 trials and 93 measurements are summarized in Figure 9. As with the effects of the crystal temperature, the data involving the laser temperature is not conducive to a single simple function, but it shows Gaussian character near the maximum power.

$$\delta\lambda = \frac{0.4429\lambda}{L} \left| \frac{n_{780} - n_{1560}}{\lambda} + \frac{\partial n_{1560}}{\partial \lambda} - \frac{1}{2} \frac{\partial n_{780}}{\partial \lambda} \right|^{-1} \quad (25)$$

Similarly to the Crystal Temperature investigation, the FWHM calculated by Fejer et al. for the wavelength is given by Equation 25. At $\lambda = 1560$ nm, the predicted FWHM is:

$$\delta\lambda = 0.288 \text{ nm} \quad (26)$$

Moreover, our experimental results indicate:

$$\delta\lambda = 0.299 \pm 0.003 \text{ nm} \quad (27)$$

Which is consistent with the theoretical prediction.

IV. DISCUSSION

The dependence of second harmonic power on the parameters of interest can be predicted from the amplitude of second harmonic light given by Equation 16 for

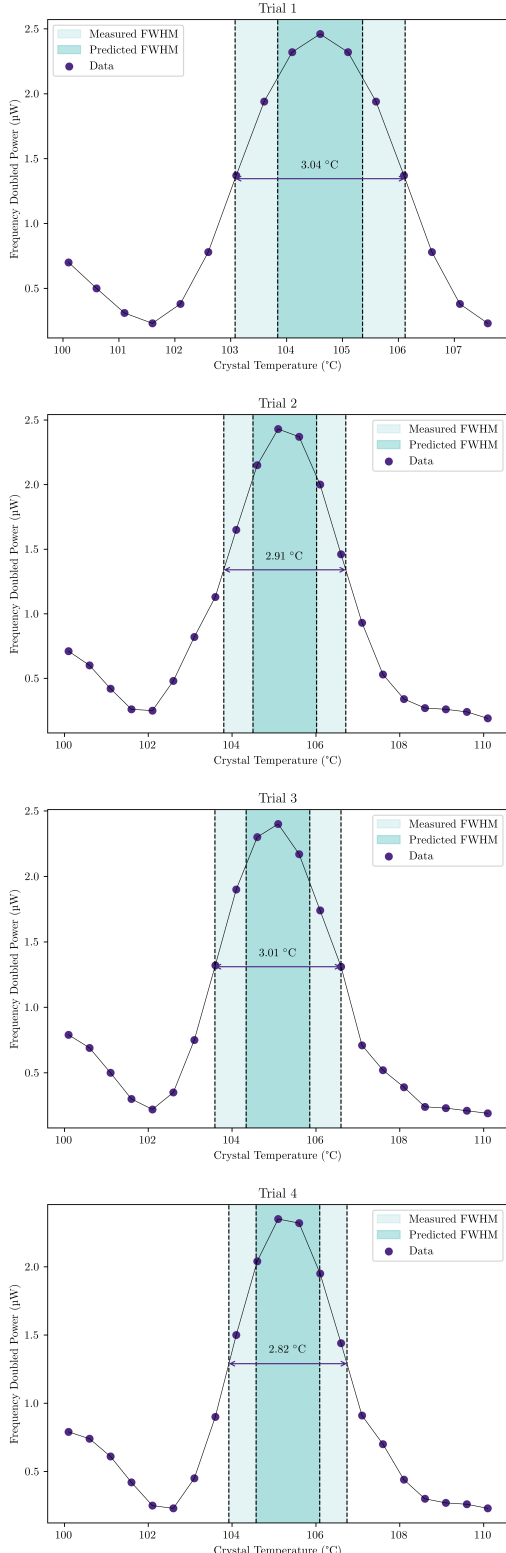


FIG. 8: Data and FWHM for the Gaussian region of the plots. Predicted FWHM calculations used Equations 18 and 22. Each plot represents one of the four trials.

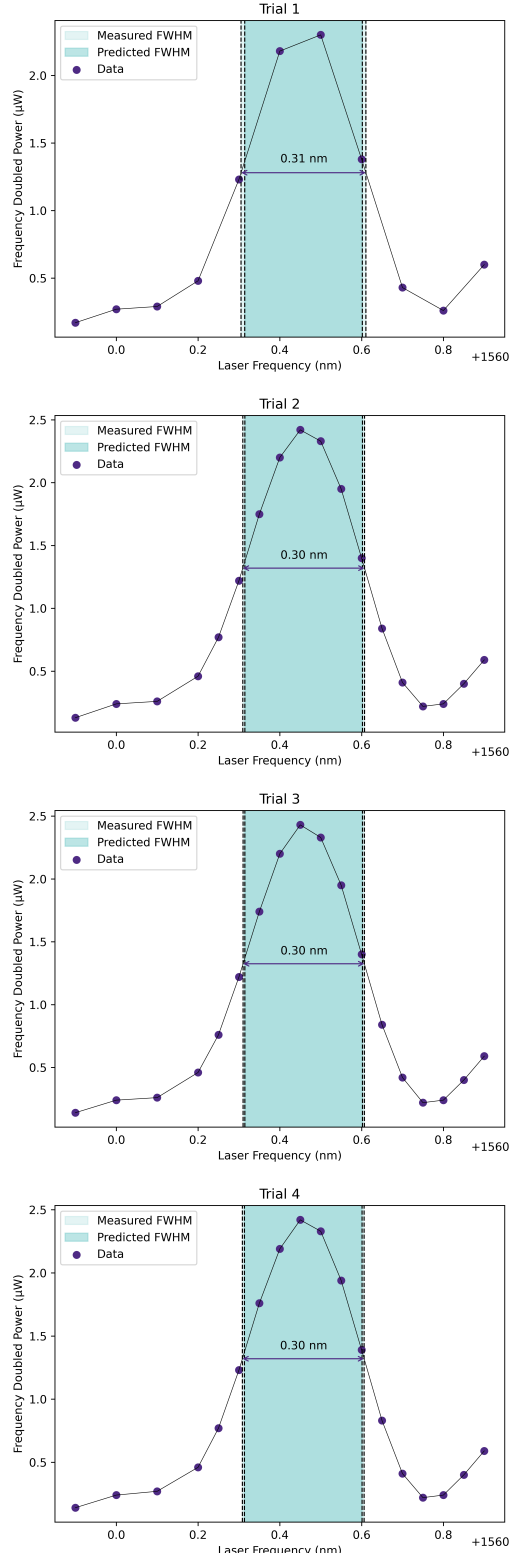


FIG. 9: Data and FWHM for the Gaussian region of the plots. λ is the wavelength offset from an estimated 1560 nm at 21.00 °C. Predicted FWHM calculations used Equations 18 and 25. Each plot represents one of the four trials.

$m = 1$, since the PPLN crystal is first-order quasi-phase matched, with the wavevectors $k_1 = n_1\omega_1/c$ determined by the indices of refraction, which in turn are given by the Sellmeier equation (18). The accuracy of all the data is impacted by the assumption in the theory that the laser is uniform through the length of the PPLN crystal. In fact, it is focused, becoming narrowest at the center of the crystal, giving the crystal an effective length less than its physical 40 mm length. Another assumption is that the diode laser is perfectly monochromatic. Other factors limiting the accuracy of all data include the amount of data collected, slight shifts in background light affecting measurements of power, and the high sensitivity of the power meters.

Although the sensitivity of the power meters is conducive to precise measurements, it also leads to variations in power measurements in ways conflicting with theoretical predictions. An example is rapidly turning the waveplate several full rotations so that the waveplate returns to its original orientation. Despite the fact that angle remains the same before and after the rotations, the power that is measured will be significantly different, owing to this high sensitivity.

A. Angle Dependence

The angle of the linearly polarized light exiting the half waveplate is twice the angle of the waveplate. As previously mentioned, the PPLN crystal is designed to output second harmonic light in proportion to the vertical component $|E_1 \cos 2\theta|$ of the incident light, where θ is the waveplate angle. The amplitude of the second harmonic light, being produced by a second-order polarization due to this vertical component, is then proportional to $(E_1 \cos 2\theta)^2$. Finally, the power measured by the power meter is quadratically related to the SHG amplitude. The theoretical prediction for the angle dependence of second harmonic power is then

$$Q(\theta) = K_\theta \cos^4(2\theta) \quad (28)$$

where Q is the power and K_θ is a constant involving the frequencies, coefficients and length of the PPLN crystal, and the fourth power of the amplitude of the incident light.

The results of the experiment are consistent with this theory insofar as the angle dependence is best represented as the fourth power of a sinusoidal function. This type of function matched the data significantly more closely than other even exponents of the sine function. The experimental angle dependence equation is

$$Q(\theta) = 2.23 \sin^4(2.02\theta - 1.49) \quad (29)$$

where Q is in μW and θ is in radians. The coefficients have uncertainties given by 2.23 ± 0.02 , 2.02 ± 0.01 , and -1.49 ± 0.02 , respectively.

This equation is consistent with the theoretical prediction from Equation 28, with the phase of the function

being slightly different (1.49 compared to the expected 1.57 radians) and the B term slightly above the expected 2.00. Higher amplitudes for power, as have been seen in the laser current and temperature measurements, are possible for this apparatus, but since the angle was the first parameter measured, temperature optimizations had not yet been determined. It was found that the 24.20 degree laser temperature was sub-optimal for the oven temperature and current during the angle dependence measurements. The precision of waveplate angle selection was limited to 2 degrees, the interval at which each mark on the waveplate was placed.

B. Laser Current and Input Power Dependence

Aside from the effect of the laser current on its frequency, theory predicts a quadratic relation between the amplitude and the power of the 1560 nm light as it exits the PPLN crystal $Q_{\text{in}} \propto A_1^2$, and since $A_2 \propto A_1^2$, the power of second harmonic light $Q_{\text{out}} \propto A_2^2$ is proportional to the square of the power of 1560 nm light.

$$Q_{\text{out}} \propto Q_{\text{in}}^2 \quad (30)$$

The dependence of laser amplitude on the driving current is complex. Of course, it is reasonable to predict that increases in current lead to increases in amplitude, and this has been experimentally shown, but the precise relation is unknown. The guess used to model the data in Figure 7

$$Q_{\text{out}} \propto I_{\text{in}}^4 \quad (31)$$

follows from the largely random assumption that $A_1 \propto I_{\text{in}}$. The experimental current dependence of second harmonic power (Figure 7) is inconsistent with the prediction in Equation 31. As previously mentioned, the drift in laser frequency with changes to current is the primary cause. As seen in Figure 9, the frequency drift introduces an approximately Gaussian element to the relation, so the data in Figure 7 is the result of some unknown relation between laser amplitude and current, combined with the (mostly) Gaussian wavelength dependence.

The experimental results in Figure 6 match the theory and show high internal consistency. Attempting to model the data with cubic and quartic functions resulted in quadratic coefficients much higher than the cubic or quartic, so it is evident the data matches the prediction of Equation 30. The average of the quadratic fit equations relates the output power to the input power as

$$Q_{\text{out}} = (0.012541 \pm 0.000002)Q_{\text{in}}^2 \quad (32)$$

where Q_{out} is in μW and Q_{in} in mW. The accuracy of these measurements is limited by the different ending locations for the 1560 nm and 780 nm light, which may have lead to a slight difference in background light between the two locations. Of course, the influence of

current on frequency is also an accuracy-limiting factor that may not have been completely compensated for by the adjustments in temperature. Another difficulty with parameters affecting frequency is the fact that it is unknown exactly how deviations of the wavelengths from those specified on the power meter affect the amount of power detected.

C. PPLN Crystal Temperature

Deviations from ideal QPM conditions lead to suboptimal power output in SHG [9]. For example, adjusting the temperature of the crystal results in different refractive indexes for the travelling light, which in turn affects the coherence length described in Equation 13. Moreover, thermal expansion affects the period Λ and length L of the crystal. Since these parameters must follow very strict relationships for QPM to work, determining the tuning properties and acceptance bandwidth for temperature in SHG is critical if we want to maximize the frequency doubled power.

In our experiment, we found that the FWHM was $\delta T = 2.9 \pm 0.1$ °C. On the other hand, using theoretical predictions from Equation 24 we would expect $\delta T = 1.51$ °C. This difference could be explained by the fact that theory assumes the laser propagates as a plane wave, while in reality the envelope is closer to a gaussian beam. In other words, the power away from the center of the crystal is much weaker than we estimate it to be, so there's a larger margin for temperature variations that will not impact the total power output very much. Another effect that might account for some of this difference is the possibility that we didn't wait enough time for the crystal to thermalize after changing its temperature. We might have recorded a larger temperature variation than what the crystal actually went through. We believe, however, this would account for a minimal contribution given that we always waited until the output power was reasonably stable before recording its value.

D. Laser Temperature and Frequency

Similarly to how crystal temperature can affect the QPM conditions, changing the fundamental wavelength of the laser λ will affect the indexes of refraction directly, and phase matching will not be ideal. Across all 4 trials, we measured the FWHM related to wavelength consistently, resulting in the experimental value of $\delta\lambda = 0.299 \pm 0.003$ nm. This is in good agreement with the expected $\delta\lambda = 0.288$ nm, although it's outside the uncertainty interval that we calculated. Beyond system-

atic errors and the problems with the plane assumption we discussed, one possible reason for the slight disagreement is that in the derivation of Equation 25, Fejer et al. expand Δk as a function of λ , but they drop all terms with order higher than 1. It's possible that the contribution from these terms is significant enough to generate the small disagreement between experiment and theory.

V. CONCLUSION

In this experiment, we observed SHG from a PPLN crystal excited by a 1560 nm laser. We have investigated the phenomena from different perspectives, and confirmed with reasonable certainty that various theoretical predictions were correct. Each of our 5 experiments yielded a final expression that summarizes the data.

Polarization Angle Dependence:

$$Q(\theta) = 2.23 \sin^4(2.02\theta - 1.49) \quad (33)$$

Input Power Dependence:

$$Q_{\text{out}} = (0.012541 \pm 0.000002)Q_{\text{in}}^2 \quad (34)$$

Crystal Temperature Bandwidth:

$$\delta T = 2.9 \pm 0.1 \text{ } ^\circ\text{C} \quad (35)$$

Laser Wavelength Bandwidth:

$$\delta\lambda = 0.299 \pm 0.003 \text{ nm} \quad (36)$$

Using these equations we validated that: 1) the frequency doubled power depends on the fourth power of the sine of the polarization angle; 2) the frequency doubled power depends on the square of the input power; 3) the laser frequency acceptance bandwidth is approximately given by Equation 25. We also had results regarding the crystal temperature dependence, and although the theoretical predictions were close, there was significant difference between the two. Perhaps, the theoretical derivations would be more accurate if we made them under the assumption of a gaussian beam. Waiting more time for the crystal to thermalize after changing its temperature could also improve the results. In addition to that, we could make a better use of the data collected on the laser current dependence investigation if we had a model of the frequency drifting aspect. In this sense, a better mathematical description would improve our methodology. Beyond these improvements, it is clear that collecting more data would allow for more statistical significance. Moreover, being mindful of the impacts of background lighting and proper handling of the equipment could help reducing systematic errors. This is especially true for the angle dependence data, in which we had some trouble keeping the waveplate in place.

-
- [1] Kimbell Art Museum. *Art and empire*. Harry N. Abrams, New York, NY, September 1995.
- [2] Johannes Kepler. *Optics*. Green Lion Press, Santa Fe, NM, November 2000.
- [3] Isaac Newton. *Opticks*. Dover Books on Physics. Dover Publications, Mineola, NY, June 1952.
- [4] James Clerk Maxwell. Viii. a dynamical theory of the electromagnetic field. *Philosophical Transactions of the Royal Society of London*, 155:459–512, 1865.
- [5] Jeff Hecht. *Beam*. Oxford University Press, New York, NY, May 2010.
- [6] Robert W. Boyd. *Nonlinear Optics*. Academic Press, Burlington, third edition, 2008.
- [7] Note that Einstein’s summation convention is in use.
- [8] Note that we assume the medium responds instantaneously to variations in the electric field.
- [9] Martin M. Fejer, G. A. Magel, Dieter H. Jundt, and Robert L. Byer. Quasi-phase-matched second harmonic generation: tuning and tolerances. *IEEE Journal of Quantum Electronics*, 28(11):2631–2654, 1992.
- [10] Mark A. Kasevich, Tim Kovachy, Alex Sugarbaker, Remy Notermans, Peter Asenbaum, Chris Overstreet, and Jason M. Hogan. Macroscopic scale atom interferometers: Introduction, techniques, and applications. 2017.
- [11] <https://covesion.com/en/resource/material-properties-of-lithium-niobate/>.